Int. J. Heat Mass Transfer. Vol. 34, No. 3, pp. 633–647, 1991
Printed in Great Britain

0017–9310/91 $3.00+0.00

Forward and inverse analysis of single and multiple scattering of collimated radiation in an axisymmetric system

BIRENDRA M. AGARWAL and M. PINAR MENGÜÇ
Department of Mechanical Engineering, University of Kentucky, Lexington, KY 40506, U.S.A.

(*Received* 19 *June* 1989 *and in final form* 23 *March* 1990)

Abstract—In this work, scattering of a collimated light source incident on a single/multiple scattering axisymmetric medium is studied and the extent to which analysis can be used to recover the effective radiative properties of the medium is determined. For this purpose, a He–Ne laser nephelometer is designed and the angular scattered intensity distributions measured in the single and multiple scattering regimes for mono- and polydispersed suspensions of particles. Analytical expressions are derived for the angular intensity distribution, accounting for up to two successive scatters. The experiments show very good agreement with the theoretical calculations. Also, an inverse analysis is presented to determine the phase function coefficients of particles *in situ* using the experimental results. The first two coefficients of the Legendre expansion of the phase function are recovered for both mono- and polydispersions within 10% of the actual value for experiments conducted at low optical thicknesses ($\tau < 0.5$).

INTRODUCTION

THE PROPAGATION of radiation through a participating medium has been the focus of a large number of diverse studies, including atmospheric sciences, remote sensing, meteorology, astrophysics, biology, medicine, laser diagnostics, and radiation heat transfer. Laser diagnostic techniques have been used in the past for flow visualization, determining volume compositions, temperature and concentration distributions, particle sizes, and for flame studies to investigate soot formation as well as turbulence–radiation interactions. A detailed review of these applications is available [1].

Understanding the propagation of light through a participating medium is critical in determining the radiative properties inside practical systems, such as combustion chambers, diffusion and pulverized-coal flames, rocket plumes or sprays. It has recently been noted that the accurate knowledge of the radiative properties of the combustion products is currently the most critical factor in performing accurate radiative transfer predictions in combustion systems [2]. The radiative and physical property distributions in these types of systems can be obtained by coupling laser diagnostic techniques with inverse radiation transfer models.

A detailed discussion of studies related to light scattering and optical diagnostic techniques were given in ref. [3]. Most of the previous works in this area have been either for planar [4–27] or for homogeneous cylindrical systems [28–35]. Although some of these studies dealt with determining the phase function of the scatterers [6, 23, 28–34], the effects of multiple scattering and medium inhomogeneity on the angular scattered intensity distribution have not been investigated extensively. A summary of the experimental studies dealing with light propagation in participating media is shown in Table 1. Although, most of the experimental works included in this table were performed using latex particles, other types of scatterers including teflon particles [13], non-spherical sodium chloride and potassium sulfate particles [29], algal suspensions [30–32], titanium dioxide and pigments [18], polymer [19], carbon black [20], and fly ash particles [34] were also employed.

For modeling of radiation heat transfer in combustion systems, we need to know the radiative properties of particles, which are usually irregular shaped and nonhomogeneous. It is difficult, if not impossible, to determine their radiative properties from theory, due to the lack of appropriate theoretical models and particle shape and optical property (spectral complex index of refraction) data. Our primary research interest is the determination of the radiative properties of these type of particles in axisymmetric cylindrical media *in situ* using optical diagnostic techniques.

In this study, we will concentrate our efforts on homogeneous and spherical mono- and polydispersed latex particle clouds. The reason for using these types of particles is two-fold: we know the complex index of refraction of latex at He–Ne laser wavelength, and because these particles are spherical in shape, we can use the Lorentz–Mie theory to predict their radiative properties accurately. Therefore, we can generate a theoretical data base to compare against the experimental results. If we can show that the radiative properties obtained from experiments are in good agreement with the theoretical predictions, then we can employ the same type of experiments to determine the radiative properties of irregular shaped non-homo-

NOMENCLATURE

a	Legendre coefficients of the phase function expansion, equation (15)
d	diameter [μm]
$\bar{d}$	mean diameter [μm]
f_v	volume fraction [$m^3 m^{-3}$]
I	intensity [$W m^{-2} sr^{-1}$]
k	imaginary part of the index of refraction
l	physical length [m]
L	physical length [m]
n	real part of the index of refraction
$\tilde{n}$	complex index of refraction, $n-ik$
P_k	Legendre polynomial of order k
Q	efficiency factor for absorption, extinction and scattering
s	path of radiation
x	size parameter, $\pi d/\lambda$.

Greek symbols

α	polar scattering angle (see Fig. 1)
β	extinction coefficient [m^{-1}]
θ	polar scattering angle (see Fig. 1)
κ	absorption coefficient [m^{-1}]
λ	wavelength [μm]
σ	scattering coefficient [m^{-1}]
τ	optical thickness
Φ	scattering phase function
Ω	direction of propagation.

Subscripts

1	first-order scattering
2	second-order scattering
a	absorption
e	extinction
m	monodisperse
p	polydisperse
s	scattering.

geneous particulates, such as pulverized-coal/char particles and soot agglomerates.

In the paper, a coupled analytical and experimental study is presented to develop a basis for the determination of effective radiative properties of scattering particles subjected to a collimated incident radiation. A theoretical analysis is given to determine the angular intensity distribution at the periphery of an axisymmetric medium. Details of the experiments performed using six types of monodispersions and three polydispersions are described. Effects of particle size, size distribution, optical thickness of medium on the angular intensity distribution are discussed. An inverse analysis is employed to recover the coefficients of the Legendre polynomial expansion of the scattering phase function of particles from the experimental data.

ANALYTICAL FORMULATION

For a single scattering axisymmetric medium subjected to collimated irradiation, the radiation intensity along the line-of-sight is given as

$$I = I_0 \exp\left[-\int_0^s \left(\kappa(s')+\sigma(s') - \sigma(s')\frac{\Phi(0,s')\Delta\Omega}{4\pi}\right)ds'\right] \quad (1)$$

where I_0 is the intensity of the incident radiation at the boundary, and κ and σ the spatially and spectrally dependent absorption and scattering coefficients along the path s, $\Phi(0, s')$ is the scattering phase function in the forward direction, $\Delta\Omega$ the small finite solid angle in the forward direction and s' the dummy spatial variable. For the sake of simplicity, the wavelength dependency of the radiative properties and intensity is not shown explicitly, but it is understood. The first two terms in the exponent determine how much radiation is attenuated by the medium along the line-of-sight. The third term in the exponent on the right-hand side of equation (1) is the in-scattering gain due to the scattering in the forward direction. In-scattering contribution from all possible directions is not considered in this expression because of the single scattering approximation. However, if the optical thickness of the medium increases, multiple scattering effects become important and they must be accounted for. The emission contribution is not considered in equation (1) either, since our focus here is on the absorption and scattering of incident radiation by the medium. Experiments can be performed by modulating the incident light source using a beam chopper and a lock-in amplifier; therefore, effects due to all continuous radiation sources, including the medium emission, can be eliminated.

First-order scattering

Let us consider here only the first-order scattering. The geometry of the physical system being considered is shown in Fig. 1(a). Let I_0 be the intensity at point P′ where the laser light enters the scattering medium. Let the detector be placed at an angle θ to the incident direction of the beam at the center O. The detector views a portion of the beam length because the solid angle of detection is finite and the length of the beam viewed depends on the angle θ and the solid angle of detection. Let P_1 and P_2 be the limits of the field of view of the detector on the laser beam. Here, we assume that the detectors receive only the energy scattered by the particles within the plane of the laser

Table 1. Experiments in light scattering

Year	Reference	Scattering medium	Property measured	Character of medium	Parameters investigated	Major findings
1961	Dezelic and Kratohvil	Uniform polystyrene latex spheres in distilled water; $d = 0.035$–$1.171\ \mu m$	Transmission, polarization ratio, dissymmetry, angular scattering	$1.199 < n < 1.214$ $0.48 < x < 9.09$	$\theta, \Phi(\theta), x$	Mie theory can be applied to the light scattering of latex particles. Measurements give diameters lower than those from electron microscopy.
1964	Woodward	Uniform polystyrene latex spheres in distilled water	Angular scattered intensity distribution	$n = 1.2$ $x = 22.2, 16.5$	x, τ	The Hartel multiple scattering theory is verified experimentally using fairly high concentration of spherical latex particles.
1965	Kratohvil and Smart	Uniform polystyrene latex spheres in distilled water; $d = 1.171$ and $1.305\ \mu m$	Absolute angular scattered intensity distribution	$n = 1.199$ $x \cong 8$–12	p^* and effect of solid angle	Polarization effects are not important. Reflections from cell wall must be accounted for.
1965	Smart *et al.*	Polystyrene latex spheres	Multiple scattering effects	$n = 1.194$ $x = 7.35; 9.2$	θ, τ, x	Experimental results for multiple scattering matched closely with those obtained from the Hartel theory.
1968	Sarofim *et al.*	Uniform polyvinyl toluene spheres painted on a glass slide; $d = 3.49\ \mu m$	Bidirectional transmission	$9.56 < x < 25.16$ $1.56 < n < 1.61$	θ, p^*, x	Particles can be treated as Mie scatterers except in a 20° cone in the direction of forward scattering.
1970	Phillips *et al.*	A single polystyrene latex particle suspended in an electric field; $d = 1.099\ \mu m$	Differential scattered intensity for vertically and horizontally polarized light	$x = 6.7106$ $n = 1.59$	θ, p^*	A method to determine optical parameters of single particles showed disagreement with particle size quoted by manufacturer.
1971	Hottel *et al.*	Uniform polystyrene latex spheres in distilled water; $d = 0.102$–$0.530\ \mu m$	Bidirectional transmission and reflection	$0.764 < x < 3.05$ $1.14 < n < 1.20$ $0.01 < \tau < 3211$	θ, x, τ	A correlation is given to accommodate the variation in effective scattering cross sections of close-packed media for clearance $> 0.3\lambda$ and $> 0.4d$.
1972	Querfield *et al.*	Uniform polystyrene latex spheres in distilled water; $d = 0.245\ \mu m$	Bidirectional transmission and reflection	$x = 1.875; 2.348$ $n = 1.194$ $0.05 < \tau < 1.2$	θ, p^*, x, τ	Experimental arrangement can be used as an analog computer for systems for which theory is intractable.
1972	Margolis *et al.*	Uniform polystyrene latex spheres in distilled water; $d = 0.109$ and $1.30\ \mu m$	Reflection in normal direction	$x = 1.09; 11.03$ $n = 1.194$	x, τ, ω	Technique to study behavior of cloudy planetary atmospheres.
1972	Granatstein *et al.*	Polydispersed teflon spheres in distilled water; $d < 0.4\ \mu m$	Reflection at $\theta = 180°$ for $\theta_{in} = 24°$	$0.264 < x < 2.64$ $n^2 = 1.89 + 0.002i$	ω	Successful theoretical model for multiple scattering of light by a turbid medium.
1973	Cohen *et al.*	Polyvinyl toluene latex spheres in distilled water; $d = 1.305$, 2.051 and $2.956\ \mu m$	Scattered intensity at $\theta = 90°$	$n = 1.18$ $17.4 < x < 42.4$	x, λ	Experimental measurements agree with theory if index of refraction provided by the manufacturer is correct.

Table 1.—*Continued*

Year	Reference	Scattering medium	Property measured	Character of medium	Parameters investigated	Major findings
1975	Colby *et al.*	Uniform polystyrene latex spheres in distilled water; $d = 0.312$, 0.481 and 0.794 μm	Angular scattered intensity distribution	$n = 1.199$ $x = 2.06$, 3.18, 5.24	x, τ	Deviations from Mie pattern are obtained for dense suspensions. Relaxation time for multiple scattering is much smaller than that obtained from a single scattering model.
1975	Graber and Cohen	Latex spheres suspended in water; $d = 3.0$ μm	Scattered intensity at $\theta = 90^\circ$	$n = 1.20$ $N = 1.11 \times 10^5$ and 3.55×10^6 cm^{-3}	τ, x, λ	Three orders of scattering are sufficient to explain multiple scattering up to an optical depth of about 1.8.
1975	Leader and Dalton	Uniform polystyrene latex spheres in distilled water; $d = 0.109$ μm	Reflection at $\theta = 0$–60° for $\theta_{in} = 35^\circ$	$x = 0.54$ $n = 1.194$	ω	Good comparison of theory with experiment for $\tau = 1.0$ and 10.0. Discrepancies for $\tau = 0.1$.
1976	Marshall *et al.*	Polystyrene latex spheres; $d =$ 0.3–11.0 μm	Angular scattered intensity distribution	$n = 1.199$ $x = 1.49$–54.6	θ, x	Unique design for a photometer to measure a 360° scattering pattern can be used to characterize a size distribution of latex particles.
1976	Pinnick *et al.*	Non-spherical particles of sodium chloride and potassium sulfate	Angular scattered intensity distribution	$n = 1.54$; 1.49 $3 < x < 10$	θ, p*	For $x < 5$ results match Mie theory, but for $x > 5$ the light intensity is more in the forward scattering lobe and less at other angles as compared to values from Mie theory.
1978	Daniel *et al.*	Unicellular algal suspensions	Angular radiation intensity and radiative flux	$d_{mean} = 3$ μm $\beta = 0.02$ m^{-1}	τ, θ	Experimental data correlate well with calculations based on discrete ordinates method and six-flux model, but deviates from results obtained using two-flux and Beer's law models
1978	Privoznik *et al.*	Unicellular algal suspensions	Extinction and absorption cross sections and the scattering phase function	Bimodal distribution with peaks at $d = 1.0$ and 2.8 μm	λ, θ	The scattering phase function is strongly peaked in the forward direction. The absorption cross section shows wavelength dependence and increases with cell size and pigment content.
1978	Look *et al.*	Mixture of latex, titanium dioxide and pigment	Back-scattered intensity	$C_s/V = 83.9$ m^{-1}	τ	The intensity leaving the media can be expressed as a function of the optical radius.
1978	Spinrad *et al.*	Spherical particles of a copolymer of styrene and divinyl benzene suspended in water; $d_{mean} = 5.2$, 8.0 and 9.8 μm	Volume scattering function at near-forward angles	$n = 1.15$ $x_{mean} = 25.8$, 39.7 and 48.7	$I(\theta)$ for $0^\circ < \theta < 1^\circ$	The effect of the unscattered main beam can be removed when making scattering measurements at near-forward angles.
1979	Incropera and Privoznik	Waste water suspension and symbiotic algal culture	Extinction and absorption cross sections and the scattering phase function	d_{mean} (waste water) = 1.11 μm d_{mean} (mature algal culture) = 1.85 μm	λ, θ	Scattering dominates extinction. Cross sections for algal cultures are six times those for waste water. Phase function has strong peak in forward direction for both cases.
1980	Bartholdi *et al.*	Latex particles; $d = 1.1$–19.5 μm	Angular scattered intensity distribution	$n = 1.20$ $8.9 < x < 159.0$	$I(\theta)$, θ	A light scattering photometer to make measurements for $\theta = 2.5$–177.5° can be used to determine the composition of a mixture of latex particles of different sizes.

Table 1.—*Continued*

Year	Reference	Scattering medium	Property measured	Character of medium	Parameters investigated	Major findings
1980	Janzen	Carbon black	Dimensionless extinction cross section	$1.72 < n < 2.13$ $0.16 < x < 3$	λ, n	Extinction spectra for dilute carbon black sols are fitted precisely by Mie theory for ensembles of spheres.
1981	Look *et al.*	Latex particles in a water solution; $d = 0.03$ 1.011 μm	Back-scattered radiation	$0.1 < \tau < 10$ $0.26 < x < 25$ $n = 1.20$	θ, τ	Influence of anisotropic scattering shifts the maximum of the radial distribution of scattered intensity to larger optical radii as the particle size increases.
1981(a)	Nelson	Uniform polystyrene latex spheres in distilled water; $d = 0.481$ μm	Angular scattered intensity distribution	$n = 1.2$ $x = 3.11, 3.69, 4.64$	λ, θ	Good agreement between experiments and Mie theory shows that latex particles can be used for controlled laboratory radiation scattering experiments.
1981(b)	Nelson	Uniform polystyrene latex spheres in distilled water; $d = 0.109, 0.481,$ 1.011 μm	Radiative scattering cross section	$n = 1.2$ $x = 0.65$–11.19	C_s, x	The scattering particle distribution function and concentration, as well as the scattering coefficient, can be obtained by comparing experimental and theoretical values of the radiative scattering cross sections.
1986	Battistelli *et al.*	Uniform latex spheres in distilled water; $d = 0.30, 0.110, 15.7$ and 5.76 μm	Forward scattered intensity and transmission	$n = 1.59, 1.53$ $x = 1.98, 7.27, 103.8$ and 37.7	$I(\theta)$ for $\theta < 3^\circ$, τ, x	A transmissometer design with variable field of view can be used to separate the forward scattered power from transmission measurements. Double scattering is sufficient to explain results for $\tau < 1.5$.
1986	Nelson *et al.*	Latex particles in a water solution; $d = 0.046$–0.35 μm	Back-scattered radiation	$0.3 < x < 2.31$ $n = 1.195$	$\tau, \omega, \Phi(\theta)$	Back-scattered radiation in optically thick media is very sensitive to changes in ω, when ω is near 1.
1987	Gerstl *et al.*	Latex spheres suspended in water; $d = 2.26$ μm	Off-axis forward scattered radiation	$n = 1.2$, $x = 14.92$	τ	The effect of the field of view of the detector in forward scattering measurements. Calculations are improved by coupling the small-angle approximation with diffusion theory.
1987	Boothroyd *et al.*	Fly ash particles	Angular scattered intensity distribution	$n = 1.5$–0.012i $x_{mean} \cong 33$	$\Phi(\theta)$	Fly ash can be treated as spherical particles under furnace conditions.
1987	Nelson and Satish	Uniform polystyrene latex spheres in distilled water; $d = 0.481$ μm	Transmission of laser beam through a multiple scattering medium	$n = 1.194$ $x = 3.18$	τ	Anisotropic scattering data correlates with scattering theory for optical thicknesses of 2.0–10.0.
1988	Nelson and Satish	Uniform polystyrene latex spheres in distilled water; $d = 0.091$ and 0.481 μm	Radial scattering	$n = 1.197$ $x = 0.601, 3.178$	τ, x	Single scattering approximation holds for optical depth up to 0.4 if depth-to-diameter ratio is unity.
1991	Agarwal and Mengüç (present study)	Uniform polystyrene latex spheres in distilled water; $d = 0.091, 0.300$ 0.482, 0.720, 0.966 and 3.06 μm; polydispersions	Scattering phase function	$n = 1.199$ $0.6 < x < 20.2$	$\Phi(\theta), x, \tau$	If two orders of scattering are accounted for, single and multiple scattering measurements for mono- and polydispersions of particles show good agreement with theory until an optical thickness of 1.0 is reached. First two phase function coefficients are recovered accurately.

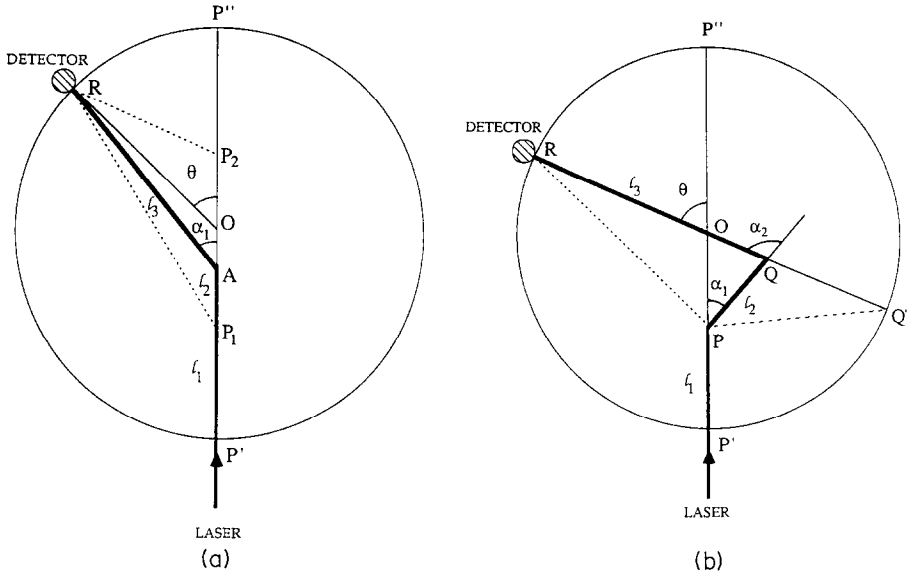

FIG. 1. Geometry and nomenclature for successive scattering in homogeneous, cylindrical system: (a) first-order scattering contribution; (b) second-order scattering contribution.

beam and the detectors. The contribution of particles above and below this plane to the scattered intensity readings can be neglected if a small pinhole is used in the experiments to block all radiation other than that from the plane of interest. The intensity at the point P_1 along the path of the beam after attenuation along $\overline{P'P_1}(=l_1)$ is given as

$$I_{P_1} = I_0 e^{-\bar{\beta} l_1}. \tag{2}$$

Here $\bar{\beta}$ is the effective extinction coefficient of the medium and is given as

$$\bar{\beta} = \kappa + \sigma\left(1 - \frac{\Phi(0)\Delta\Omega}{4\pi}\right). \tag{3}$$

If A is any point between P_1 and P_2 which can contribute to first-order scattering of the light towards the detector, the intensity at A after attenuation along $\overline{P_1A}(=l_2)$ is written as

$$I_A = I_{P_1} e^{-\bar{\beta} l_2}. \tag{4}$$

Only a fraction of the intensity reaching A is scattered towards the detector and the intensity of light that finally reaches the detector after attenuation along $\overline{AR}(=l_3)$ is given by

$$I_R = \sigma \frac{\Phi(\alpha_1)\Delta\Omega_1}{4\pi} I_A e^{-\bar{\beta} l_3} \tag{5}$$

where σ is the scattering coefficient, $\Phi(\alpha_1)$ is the value of the scattering phase function for the scattering angle α_1 and $\Delta\Omega_1$ is the solid angle subtended by the detector at R with respect to scattering at A. Here, we assume that the value of the phase function does not change within the small $\Delta\Omega$ and is equal to the value for the scattering angle α_1.

Equation (5) gives the contribution to scattering from a single point A. However, due to the finite value of the detector solid angle, photons scattered from anywhere along the length $\overline{P_1P_2}$ will reach the detector. We must, therefore, consider the effect of every point along $\overline{P_1P_2}(=L_2)$. Then, the intensity reaching the detector is represented as

$$I_R(\theta) = I_0 \int_0^{L_2} e^{-\bar{\beta}(l_1+l_2+l_3)} \sigma \frac{\Phi(\alpha_1)\Delta\Omega_1}{4\pi} dl_2 \tag{6}$$

where the angle α_1 is dependent on l_2. This integral can be evaluated numerically using a Gaussian quadrature scheme along $\overline{P_1P_2}$.

The expression for the first-order scattering may be simplified further by accounting for only the change in the size of the scattering control volume depending on the angular location of the detector. As we move away from the forward and backward scattering angles the size of the control volume which scatters the radiation towards the detector decreases. If the detector solid angle is small, we can use a simplified expression for calculating the contribution from first-order scattering. We assume that the light is scattered from the center of the medium, O (see Fig. 1(a)), calculate the radiation intensity from the point source at O, and then account for the field of view of the detector by multiplying this intensity with the length of the laser beam, $\overline{P_1P_2}(=L_2)$, that can contribute towards scattering at any given angle. Following this, the intensity reaching the detector can be written as

$$I_R(\theta) = I_0 e^{-\bar{\beta}(L)} \sigma \frac{\Phi(\theta)\Delta\Omega_1}{4\pi} L_2(\theta) \tag{7}$$

where L_2 depends on the scattering angle, θ, and L $(=\overline{P'O}+\overline{OR})$ is the total path length travelled by the

radiation. This simplified effect is sufficient to account for the first-order scattering if the beam divergence and the detector solid angle are small.

Second-order scattering

With increasing medium optical thickness, the effect of higher order scattering contributions would become more significant. Here, we will extend our analysis to include the effect of the second-order scattering.

Let us consider the schematic of the physical system shown in Fig. 1(b). The laser beam enters the system at point P′ and leaves the system at P″. The detector is placed at an angle θ to the direction of the incident beam at the center O and its location is represented by the point R. Again, I_0 is the intensity of radiation at the point P′ where the laser light enters the scattering medium and it is assumed that the detector solid angle is small.

Then, the intensity at any point P along the path of the beam after attenuation along $\overline{P'P}(=l_1)$ can be described with equation (2). At point P, let the light be scattered at an angle α_1 with respect to the initial line of sight. If the scattered light is to reach the detector it must reach some point along $\overline{Q'R}$ after being scattered from P. This means that only the light scattered into a specific angular range, defined by the location of $\overline{Q'R}$ with respect to P, will reach the detector. If the light reaches $\overline{Q'R}$ at a point Q after attenuation along the path $\overline{PQ}(=l_2)$, the intensity at Q is given by

$$I_Q = I_P \sigma \frac{\Phi(\alpha_1)}{4\pi} e^{-\beta l_2}. \tag{8}$$

The propagation of light from this point onwards is analogous to that for the first scattering at P except for the fact that the light must be scattered at an angle α_2 with respect to $\overline{Q'R}$ and within the solid angle $\Delta\Omega_2$ for it to reach the detector. Then, the intensity of light reaching the detector at R after attenuation along $\overline{QR}(=l_3)$ is given as

$$I_R = I_Q \sigma \frac{\Phi(\alpha_2)\Delta\Omega_2}{4\pi} e^{-\beta l_3}. \tag{9}$$

Substituting equations (2) and (8) into equation (9) and accounting for second-order scattering from all points, we write the intensity reaching the detector as a result of the second-order scattering as

$$I_R(\theta) = I_0 \int_0^{L_1} \int_0^{L_3} \sigma^2 \frac{\Phi(\alpha_1)}{4\pi} \frac{\Phi(\alpha_2)\Delta\Omega_2}{4\pi} e^{-\beta(l_1+l_2+l_3)} \, dl_3 \, dl_1. \tag{10}$$

Here $\Delta\Omega_2$ is the solid angle subtended by the detector (located at R) with respect to scattering at Q; therefore it is a function of l_3. This integral can be evaluated numerically using a Gaussian quadrature scheme for points along $\overline{P'P''}$ and $\overline{Q'R}$.

In the computations for the angular intensity distribution the beam diameter is assumed to increase linearly along the length $\overline{P'P''}$. The total contribution due to two orders of scattering is to be multiplied by the beam diameter at the location (P) where the first scatter occurred. This value is then normalized with the beam area at the center (O) of the scattering medium.

EXPERIMENTS

A plan view of the experimental setup and optical rail layout used in this study are shown in Figs. 2 and 3. A Plexiglas tank (50.8 × 50.8 × 25.4 cm) with optical windows on two opposite sides was used to contain the scattering medium. The laser beam entered the tank through the first window which has a transmissivity of 96% and an antireflection coating on both sides whereas the second one was coated only on the inside. A cylindrical aluminum shield of diameter 43.2

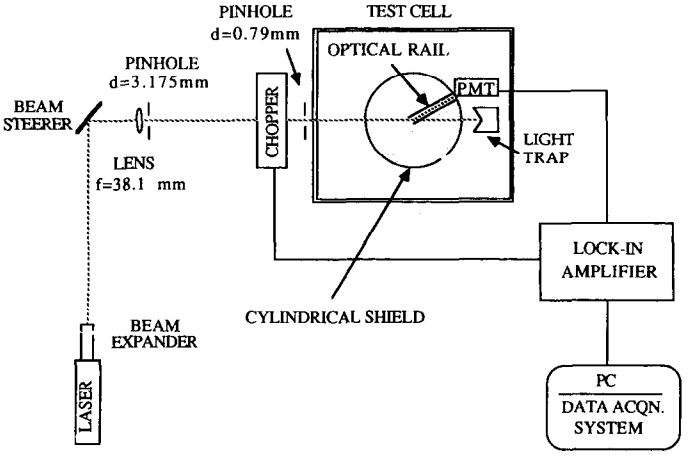

FIG. 2. Plan view of the experimental setup.

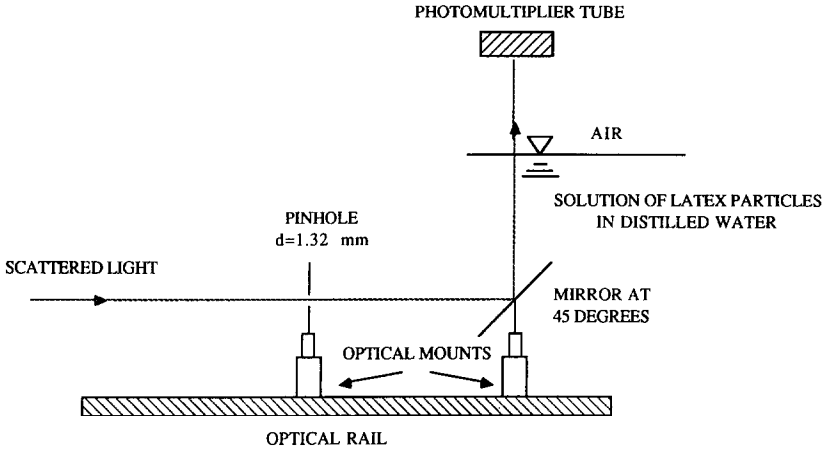

FIG. 3. Optical rail layout and the detector assembly.

cm was placed inside the tank to avoid any reflection of stray radiation from the Plexiglas tank walls. Two diametrically opposite holes of diameter 2 cm were cut in the aluminum shield to allow for passage of the light and a light trap was constructed at the further end of the shield to ensure that the beam escaped the inner cylindrical system completely and no light was reflected back into the scattering medium. The height of the cylindrical shield was greater than the water level in the tank. In the experiments, the volume inside this tank was used to calculate the optical thickness of the medium. The bottom and top of the tank, and the inside and the outside of the aluminum sheet were painted with a highly absorbing and diffusely reflecting ultra flat black paint (Krylon 1602) to avoid any reflections.

The light source used in the experiments was a 20 mW He–Ne laser (Spectra Physics, Model 106-1). A beam expander was placed just in front of the laser to allow for adjustment of the diameter of the beam entering the test cell. The beam was then directed towards the scattering medium using two planar mirrors housed in a beam steerer. A plano-convex lens and two pinholes (3.175 and 0.79 mm) were also placed in the path of the beam before it entered the test cell. The position of the lens was adjusted such that an almost parallel beam with a divergence of less than 0.5° was obtained in the scattering medium. The pinholes allowed only the center portion ($d = 3$ mm) of the 25 mm diameter laser beam to escape and this ensured that there was little or no change in the intensity across the beam. The laser light was modulated using a beam-chopper at a frequency of 150 Hz.

The detector assembly consisted of a circular base and top connected by supporting pillars. An optical rail was mounted on the base and it carried the light collection optics including the pinhole and a mirror. Because of the pinhole, the light scattered by the particles above and below the plane of the laser beam and the pinhole was not received by the detector. Therefore, the planar analysis derived in the previous section can be used to describe the physics of the problem. The top of the assembly, which housed the detector, rested on a circular groove in the cover of the tank and this allowed the whole assembly to be rotated for making measurements at various scattering angles using a single detector. The light scattered from the center of the tank reached the pinhole, placed very close to the center, and was then incident on a mirror placed at 45° to the incident direction. This arrangement was preferred to avoid any complications due to refraction effects at the water/air interface if the light is not incident in the direction perpendicular to the interface. The reflection from the water/air interface, as calculated using the standard relation $R = (n_{\text{water}} - n_{\text{air}})^2/(n_{\text{water}} + n_{\text{air}})^2$, was about 2%, and because of the low backscattering of particles used in the experiments, it did not cause any adverse effect on the detected light intensity. The mirror reflected the light upwards to the detector and in order to prevent any stray light reaching the detector the mirror was enclosed in a pipe assembly which connected the pinhole and the detector. The solid angle of detection was 6.8×10^{-4} sr. All components of the detector assembly within the tank which were exposed to the laser light were painted with the same ultra flat black paint to avoid any internal reflections within the tank.

The detector used was a photomultiplier tube (PMT; RCA, Model 4840), which was enclosed in a magnetic shield and the housing was painted with the black paint to minimize any external effects. The power supply to the detector was built in such a way that the sensitivity of the PMT could be varied to keep the output signal of the detector within the range of the sensitivity of the lock-in amplifier. The PMT converts the light signals to a voltage output signal which is fed to the lock-in amplifier. The lock-in amplifier is used to amplify the extremely low voltage signals to a range of ± 10 V, which is then input to an IBM-PC/AT through an AD board (Data Translation, Model DT2828). The data acquisition was per-

formed using the Labtech Notebook software. The data were recorded at a sampling rate of 10 Hz for 15 s. Therefore, final data points representing any reported experimental value are the average of 150 individual readings over the 15 s time interval.

The scattering medium consisted of spherical polystyrene latex particles dispersed in distilled water. These particles were spherical and uniform in size as confirmed by the electron microscope pictures [36]. The diameter of particles used were 0.091, 0.300, 0.482, 0.720, 0.966 and 3.09 μm and corresponded to size parameters from 0.6 to 20.4. The relative complex index of refraction of these particles in water is $\tilde{n} = 1.199 - i0.0$. The scattering phase functions for these particles were calculated using a Lorentz–Mie theory algorithm adapted from Dave [37].

In the experiments 150 data points were taken at each angular location and therefore a sound statistical interpretation of the data set could be obtained. A multiple-sample uncertainty analysis was used which concentrates on processing the means of sets of observations of each measured quantity [3]. The values reported on the plots are the best estimates for the result, and with 95% confidence, the true value lies within $\pm 7\%$ of that value.

RESULTS AND DISCUSSION

Experiments with monodispersed particles

Six different size monodispersed particles were analyzed. Radiative properties for the particles were obtained directly from the Lorentz–Mie theory since the particles used in this study were spherical and their size and relative refractive index ($\tilde{n} = 1.199 - i0.0$) data were available [36]. Overall, the experiments showed remarkable consistency and the results obtained agreed well with the theoretical computations.

Here, we present the results from experimental measurements and theoretical calculations for two types of particles only; $d = 0.300$ μm, $x = 1.98$ (Fig. 4) and $d = 0.720$ μm, $x = 4.75$ (Figs. 5(a) and (b)). In these figures, the normalized intensity is given in logarithmic scale; both theoretical and experimental readings at 10° are normalized to 1, 10 or 100 to include the results for up to three different τ-values in the same figure. This normalization does not change the functional form of the experimentally determined scattering diagram. If the scattering by the medium is modelled correctly using the successive scattering

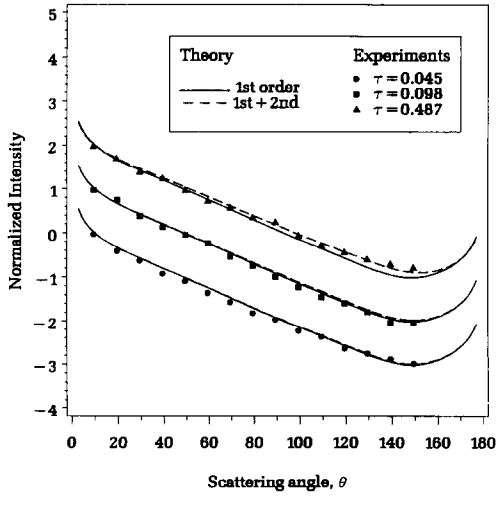

FIG. 4. Normalized angular intensity distribution for monodispersed particles; $d = 0.300$ μm. Points are the experimental data and lines are the theoretical predictions. Results are normalized at 10° to 1, 10, 100, with increasing τ, respectively. Comparisons for $\tau < 0.5$.

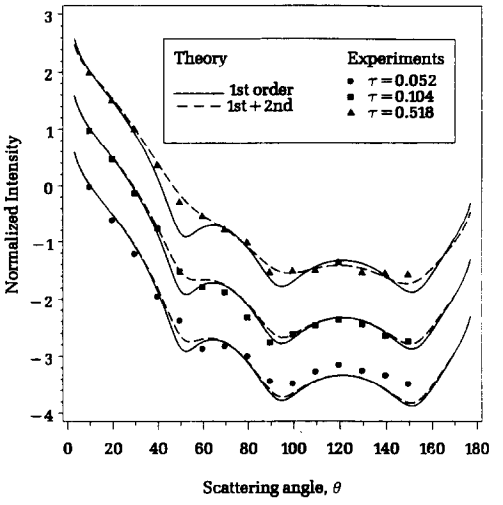

FIG. 5(a). Normalized angular intensity distribution for monodispersed particles; $d = 0.720$ μm. Points are the experimental data and lines are the theoretical predictions. Results are normalized at 10° to 1, 10, 100, with increasing τ, respectively. Comparisons for $\tau < 0.6$.

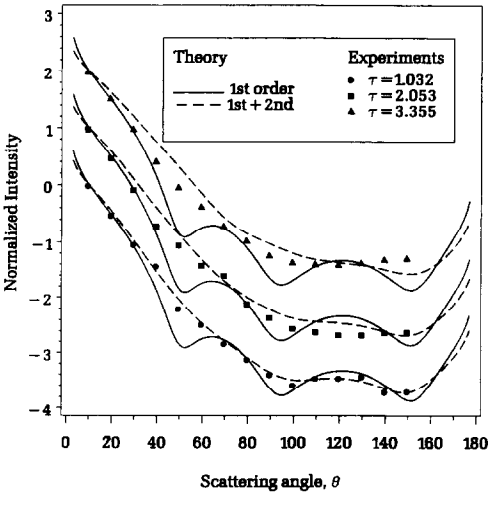

FIG. 5(b). Same as Fig. 5(a). Comparisons for $\tau > 1.0$.

approach described before, then the ratio of the experimental and theoretical intensity distributions should be equal to a constant at all angles. This constant is the calibration factor, which is a function of several effects including reflectance of the mirrors, transmittance of the window, size and power of the laser beam, sensitivity setting of the lock-in amplifier, gain of the preamplifier, characteristics of the photomultiplier tube, and water level in the test cell. By normalizing the data at 10°, we assumed a calibration factor. Then, if the experimental intensity distribution multiplied by this calibration factor matches the theoretical results at all angles, it means that the physics of the problem is adequately represented by the expressions used. With increasing optical thickness, the theory and experiments should begin to deviate, because the two orders of scattering used in the theoretical analysis may not be sufficient to describe the physical problem.

Note that at some angles the curve for the intensity including two orders of scattering lies below that for the first-order scattering because the magnitude of the 10° reading for the former is larger than the latter. No significant effect of higher order scattering contributions was observed for $\tau < 0.1$. It was noticed that the inclusion of the second-order scattering became important for higher τ values, up to ≈ 1.0, and results once again agreed well with the theory. However, if the optical thickness was further increased to values greater than 1.0, the theoretical expressions used here were not sufficient to describe the angular scattered intensity distribution accurately, especially for back scattering angles ($\theta > 120°$). The results obtained for all particles showed a similar trend [3].

Experiments with polydispersed particles

In most physical systems we encounter, the medium is composed of polydispersed particles rather than monodispersions. Therefore, it is more important to evaluate the experimental and analytical techniques with polydispersions. Three different polydispersed solutions prepared by mixing five different diameter particles were used in this study. Experiments with these arbitrary size distributions allowed us to determine if a mean diameter can be used to determine the scattering diagram of polydispersions. The compositions of these mixtures were carefully considered to have as many fluctuations in the phase functions as possible. Here, we will report the results for only one size distribution, which is composed of 0.300, 0.482, 0.720, and 0.966 μm particles with respective number densities of 5, 10, 25, and 60%. Note that this phase function yielded one of the worst agreements with the theoretical predictions.

In order to characterize the scattering medium, the first step is the defining of a mean diameter to be used for the size distribution of the particles. We calculated the properties using four different mean diameters: the arithmetic mean diameter $\bar{d}_{10}$, the mean diameter $\bar{d}_{30}^{1/3}$ based on the number density of the individual particles in the polydispersion, the Sauter mean diameter $\bar{d}_{32}$ which is based on volume to surface area ratio, and the mean diameter $\sqrt{\bar{d}_{86}}$ which appears in the scattering phase function expressions derived from Lorentz–Mie theory [38]. The definitions of these mean diameters are given as

$$\bar{d}_{mn}^{p} = \left[\frac{\Sigma_{i=1}^{n} N_i d_i^m}{\Sigma_{i=1}^{n} N_i d_i^n}\right]^p \tag{11}$$

where N_i is the number density for particles with diameter d_i.

Once a mean diameter, say $\bar{d}$, is determined, the radiative properties can be evaluated using standard procedures [2, 38, 39]. The effective extinction, absorption, or scattering efficiency factor, $\bar{Q}_e$, $\bar{Q}_a$, or $\bar{Q}_s$, can be defined as

$$\bar{Q}_\eta = \frac{\Sigma_{i=1}^{n} N_i Q_{\eta,i} d_i^2}{N_T \bar{d}^2} \tag{12}$$

where η is either for e, a or s. An effective scattering phase function, $\bar{\Phi}(\theta)$, is written as [2]

$$\bar{\Phi}(\theta) = \frac{\Sigma_{i=1}^{n} N_i Q_{s,i} d_i^2 \Phi_i(\theta)}{\Sigma_{i=1}^{n} N_i Q_{s,i} d_i^2} \tag{13}$$

where $Q_{s,i}$ is the scattering efficiency factor for the size distribution interval corresponding to the diameter d_i, and Φ_i the scattering phase function for the same interval.

The optical thickness, τ, of the polydisperse medium can be written as

$$\tau = \frac{3 f_v \bar{Q}_e L}{2\bar{d}} \tag{14}$$

where f_v is the volume fraction of the medium. Note that since we can choose any of the mean diameters mentioned earlier, for each experimental value of the volume fraction f_v, we will have a set of values for the optical thickness τ.

In comparing theoretical results with the experimental measurements, we calculated the angular scattered intensity distribution for different optical thicknesses which correspond to four different mean diameters. The smallest value of τ is based on the mean diameter $\sqrt{\bar{d}_{86}}$, the next largest value is based on the mean diameter $\bar{d}_{32}$, the still larger one based on the mean diameter $\bar{d}_{30}^{1/3}$ and the largest value of τ corresponds to the mean diameter $\bar{d}_{10}$. It is expected that the choice of mean diameter would affect the agreement between theoretical and experimental results, because τ based on $\bar{d}_{10}$ is about 50% larger than that for $\sqrt{\bar{d}_{86}}$.

In Figs. 6(a)–(c), the results for the polydispersions are depicted. The same experimental data were plotted four times in each of these figures. Both theoretical and experimental results were normalized at 10° to 1, 10, 100, or 1000 for τ values corresponding to the four different mean diameters. The trends in the results for various optical thicknesses were similar to that seen for monodispersions and other size distributions

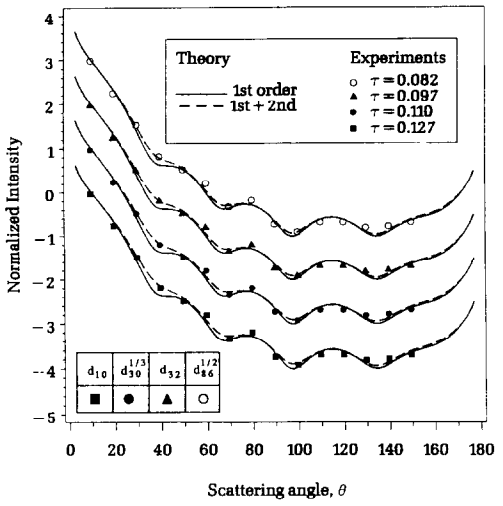

FIG. 6(a). Normalized angular intensity distribution for polydispersed particles. Points are the experimental data (same for all four plots) and lines are the theoretical predictions based on four different mean diameters. τ values are calculated from equation (14). Results are normalized at 10° to 1, 10, 100, 1000 with increasing τ, respectively. Comparisons for $\tau < 0.15$.

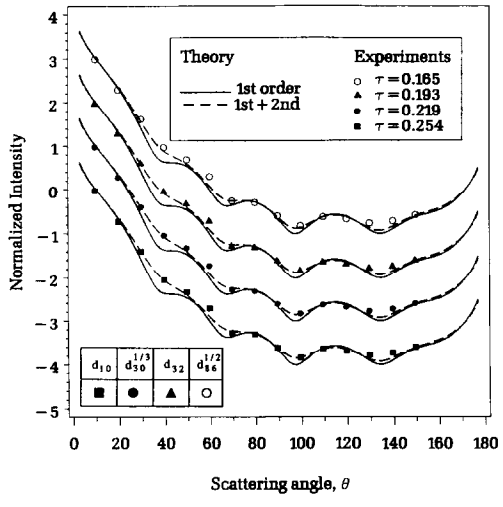

FIG. 6(b). Same as Fig. 6(a). Comparisons for $0.15 < \tau < 0.3$.

studied in the experiments [3]. Having larger size particles in the polydispersed mixture alters the intensity distribution to a great extent and the maximas and minimas become more pronounced.

An error analysis was performed to determine if one of the four mean diameters would yield a better representation of the scattering phase function than others [3]. The results showed that in determining the normalized angular intensity distribution function, any of the four mean diameters can be used. However, it should be kept in mind that $\sqrt{d_{86}}$ appears in the definition of the asymmetry factor of polydispersions

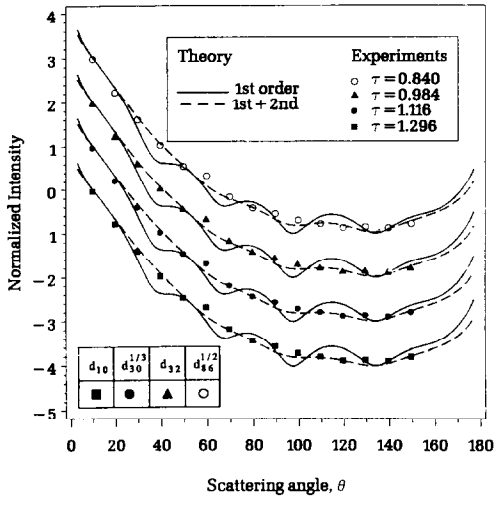

FIG. 6(c). Same as Fig. 6(a). Comparisons for $0.8 < \tau < 1.3$.

[38]; therefore, it is a natural choice for mean diameter when determining the scattering phase function.

Recovering the phase function coefficients

When we try to characterize a physical system in terms of its radiative properties, one of the important characteristics is the scattering phase function of the medium. It represents the probability that radiation propagating in a given direction is scattered into another direction because of the inhomogeneities and/or particles encountered along the path of the radiation. For most radiative transfer analyses, it is convenient to present an azimuthally symmetric phase function which can be expanded in terms of the Legendre polynomials as

$$\Phi(\cos\theta) = \sum_{k=0}^{N} a_k P_k(\cos\theta) \qquad (15)$$

where θ is the polar component of the scattering angle, that is the angle between the directions Ω' and Ω, P_k is the Legendre polynomial of degree k, and a_k the Legendre coefficients. The number of terms (N) required in the series to accurately simulate the phase function is a function of the size parameter ($x = \pi d/\lambda$) and the complex index of refraction ($\tilde{n} = n - ik$).

We attempted to recover the coefficients in the Legendre expansion of the phase functions for the mono- and polydispersions from the experimental data using an inverse analysis. Only the experimental results which correspond to low optical thicknesses were considered in the inversion, and for polydispersions $\sqrt{d_{86}}$ is chosen as the mean diameter. The measured angular scattered intensity data was modified using the simple geometrical effect discussed before (equation (7)); therefore, the effect of the scattering volume size on the intensity distribution was eliminated. The data were anchored at the 10° reading calculated from the Lorentz–Mie phase function, using the size and refractive index of latex par-

ticles supplied by the manufacturer. This is equivalent to performing experiments with 'known' particles to calibrate the optical system. The normalized data were then used to obtain the phase function coefficients using three different methods discussed in ref. [40], including a B-spline least square error fit, a step function approximation, and a delta function approximation. The last two approximations were used to determine the phase function in terms of the widely used delta-Eddington form. The B-spline fit was preferred to a simple functional fit to have a better accuracy [40].

The definitions of the step and delta phase function approximations are given as [40]

$$\Phi_s(\cos\theta) = 2f'H(\cos\theta - \cos\Delta\theta_1) + (1-f'(1-\cos\Delta\theta_1))\sum_{k=0}^{N} a'_k P_k(\cos\theta) \quad (16)$$

$$\Phi_\delta(\cos\theta) = 2f''\delta(1-\cos\theta) + (1-f'')\sum_{k=0}^{N} a''_k P_k(\cos\theta) \quad (17)$$

where δ is the Dirac delta function, H the Heavyside (step) function, f' and f'' the forward peaks of the phase functions, θ the scattering angle and $\Delta\theta_1$ the forward angular step used in the step phase function. After the a'_k and the a''_k coefficients are determined, these functions are converted into the functional form given by equation (15) [40].

We also considered a Bessel function fit to the data for the forward scattering region of angles less than 10°. The Bessel function fit is chosen based on the fact that diffraction plays an important role in forward scattering. The diffracted intensity distribution for the small forward scattering angular range is given by [41]

$$I(\theta) - I(0)\left[\frac{2J_1(x\sin\theta)}{x\sin\theta}\right]^2 \quad (18)$$

where J_1 is the Bessel function of the first kind and x the size parameter of the particle.

In most cases (except for the 0.091 μm particles where we had problems with the experiments because of impurities in the water) we could recover at least two, or in some cases more, coefficients within 10% of the actual Mie phase function coefficients (see Tables 2–4). The B-spline fit yielded remarkably accurate a_k coefficients. The procedure with the step phase function to recover the coefficients also gave acceptable results. The delta function approximation however, did not yield good results as compared to the B-spline fit results. A possible explanation for this is that the particles in our study are not highly forward scattering and the step and especially delta function approximations are more applicable for particles which have a very large forward scattering peak [40]. The procedure using the Bessel function fit yielded accurate phase function coefficients; however, the accuracy was less than that observed when the B-spline fit was used.

Table 2. Percentage error in the coefficients of the Legendre polynomial expansion of the phase function recovered from the experiments. Monodispersed particles with $d = 0.300$ μm. Fourth-order B-spline was fitted to 15 observation points. Bessel function fit was for $\theta < 10°$

	A coefficients	Error in the coefficients using B-Spline fit	Bessel function
1	0.196007E+01	1.81	3.64
2	0.147085E+01	6.11	10.14
3	0.681389E+00	12.04	24.06
4	0.226122E+00	29.39	75.14
5	0.485373E−01		
6	0.693936E−02		
7	0.700315E−03		
8	0.524709E−04		
9	0.302982E−05		

The accuracy of the recovered phase function coefficients is very promising. Based on these results, we can say that the angular scattered intensity measurement technique described here can be used successfully to recover the first two coefficients of the Legendre polynomial expansion of the scattering phase function. It has been shown recently that the radiative flux predictions based on the first two recovered phase function coefficients yielded very close agreement with those obtained using the exact, full Lorentz–Mie phase function [40]. Considering that for many systems, such as pulverized-coal flames, it is not possible to assign unique values for the complex refractive index, shape and size distribution, the analysis presented here can be readily used to obtain the fundamental phase function coefficients from similar experiments.

Although we were able to show that it is possible to recover the first two coefficients relatively accurately from experiments, we should be careful in applying these kind of experiments to different types of particles. The first two coefficients of the Legendre polynomial expansion of the phase function carry most of the information about the scattering near forward directions. Therefore, this approach is acceptable for most forward scattering particles. However, using only the first two terms of a series expansion of a complex function does not always yield accurate results. Under certain conditions, the approximate phase functions constructed from one or two coefficients yield physically unacceptable results. The user should be extremely careful about the limits of applicability of any simple phase function model before employing it to a certain system. Extensive discussions of simple phase function approximations and some remedies to avoid unacceptable predictions caused by them are given in refs. [40, 42–44].

Table 3. Percentage error in the coefficients of the Legendre polynomial expansion of the phase function recovered from the experiments. Monodispersed particles with $d = 0.720\ \mu m$. Fourth-order B-spline was fitted to 15 observation points. Bessel function fit was for $\theta < 10^\circ$

	A coefficients	Error in the coefficients using B-Spline fit	Bessel function	Step function	Delta function
1	0.266106E+01	−0.25	0.37	−0.65	−11.24
2	0.372790E+01	−1.01	−0.29	−2.01	−11.85
3	0.414407E+01	−2.89	−1.99	−4.76	−13.21
4	0.394696E+01	−5.14	−3.94	−8.27	−14.33
5	0.332291E+01	−7.24	−5.55	−12.15	−13.97
6	0.241468E+01	−7.33	−4.66	−15.08	−8.32
7	0.140533E+01	−5.12	0.03	−18.68	11.14
8	0.657514E+00	−2.57	9.45	−27.64	74.83
9	0.240345E+00	−16.15	19.12	−62.74	321.71
10	0.704893E−01				
11	0.167702E−01				
12	0.328864E−02				
13	0.540453E−03				
14	0.755492E−04				
15	0.908918E−05				

CONCLUSIONS

This work provided an insight into the forward and inverse analyses of the propagation of laser light through mono- and polydisperse particle solutions in single and multiple scattering axisymmetric systems. The experiments showed that at low optical thicknesses ($\tau < 0.2$) first-order scattering was sufficient to account for the angular scattered intensity distribution for polydispersions. Also, it was shown that the first two coefficients of the Legendre expansion of the phase function can be recovered from experiments for both mono- and polydispersions to within 10% of the actual value if the medium optical thickness is small. The results obtained from this study support the statement made by Querfield *et al.* [11] that experimental results can be used as an analog computer to determine the effective radiative properties of systems where the theory is not well documented or the medium is not well characterized in terms of its properties. Currently, we are using the approach described here to determine the phase function coefficients of pulverized-coal particles in a flame environment.

Table 4. Percentage error in the coefficients of the Legendre polynomial expansion of the phase function recovered from the experiments. Polydispersed particles; $\bar{d} = \bar{d}_{10}$. Fourth-order B-spline was fitted to 15 observation points. Bessel function fit was for $\theta < 10^\circ$

	A coefficients	Error in the coefficients using B-Spline fit	Bessel function	Step function	Delta function
1	0.273638E+01	−1.83	−4.01	−3.27	−3.79
2	0.402291E+01	−5.63	−8.07	−9.23	−9.70
3	0.479925E+01	−9.85	−12.69	−16.27	−16.69
4	0.509409E+01	−14.23	−17.61	−24.20	−24.54
5	0.497523E+01	−16.91	−21.04	−31.13	−31.36
6	0.453870E+01	−18.69	−23.90	−38.36	−38.45
7	0.383758E+01	−18.22	−25.12	−45.50	−45.37
8	0.301025E+01	−16.44	−26.05	−55.13	−54.59
9	0.215717E+01	−10.36	−24.75	−67.46	−66.15
10	0.131744E+01	7.75	−17.13	−86.99	−83.87
11	0.646407E+00	66.20	13.43	−120.19	−111.80
12	0.264055E+00				
13	0.874847E−01				
14	0.241029E−01				
15	0.561123E−02				
16	0.112222E−02				
17	0.195558E−03				
18	0.300310E−04				
19	0.409906E−05				

Acknowledgements—This research is supported by the National Science Foundation Grant No. CBT-8708679 and the Department of Energy Grant No. DE-FG22-87PC79916.

REFERENCES

1. S. S. Penner, C. P. Wang and M. Y. Bahadori, Laser diagnostics applied to combustion systems, Twentieth Symp. (Int.) on Combustion, pp. 1149–1175 (1984).
2. R. Viskanta and M. P. Mengüç, Radiation heat transfer in combustion systems, *Prog. Energy Combust. Sci.* **13**, 97–160 (1987).
3. B. M. Agarwal, An experimental and theoretical study of single and multiple scattering in an axisymmetric system, M.S. Thesis, Department of Mechanical Engineering, University of Kentucky, Lexington, Kentucky (1989).
4. G. Dezelic and J. P. Kratohvil, Determination of particle size of polystyrene latexes by light scattering, *J. Colloid Sci.* **16**, 561–580 (1961).
5. D. H. Woodward, Multiple light scattering by spherical dielectric particles, *J. Opt. Soc. Am.* **54**(11), 1325 (1964).
6. J. P. Kratohvil and C. Smart, Calibration of light scattering instruments—III. Absolute angular intensity measurements on Mie scatterers, *J. Colloid Sci.* **20**, 875–892 (1965).
7. C. Smart, R. Jacobsen, M. Kerker, J. P. Kratohvil and E. Matijevic, Experimental study of multiple light scattering, *J. Opt. Soc. Am.* **55**(8), 947 (1965).
8. A. F. Sarofim, H. C. Hottel and E. J. Fahimian, Scattering of radiation by particle layers, *AIAA J.* **6**(12), 2262–2266 (1968).
9. D. T. Phillips, P. J. Wyatt and R. M. Berkman, Measurement of the Lorentz–Mie scattering of a single particle: polystyrene latex, *J. Colloid Interface Sci.* **34**(1), 159–162 (1970).
10. H. C. Hottel, A. F. Sarofim, W. H. Dalzell and I. A. Vasalos, Optical properties of coatings: effect of pigment concentration, *AIAA J.* **9**(10), 1895–1898 (1971).
11. C. W. Querfield, M. Kerker and J. P. Kratohvil, Multiple scattering in a synthetic foggy atmosphere—experimental results, *J. Colloid Interface Sci.* **39**(3), 568–582 (1972).
12. J. S. Margolis, D. J. McCleese and G. E. Hunt, Laboratory simulation of diffuse reflectivity from a cloudy planetary atmosphere, *Appl. Optics* **11**(5), 1212–1216 (1972).
13. V. L. Granatstein, M. Rhinewine, A. M. Levine, D. L. Feinstein, M. J. Mazurowski and K. R. Piech, Multiple scattering of laser light from a turbid medium, *Appl. Optics* **11**(5), 1217–1223 (1972).
14. A. Cohen, V. E. Derr, G. T. McNie and R. E. Cupp, Measurement of Mie scattering intensities from monodispersed spherical particles as a function of wavelength, *Appl. Optics* **12**(4), 779–782 (1973).
15. P. C. Colby, L. M. Narducci, V. Bluemel and J. Baer, Light scattering measurements from dense optical systems, *Phys. Rev. A* **12**(4), 1530–1538 (1975).
16. M. Graber and A. Cohen, Multiple scattering: theoretical calculations compared with experimental dye-laser measurements, *J. Opt. Soc. Am.* **65**(11), 1306–1310 (1975).
17. J. C. Leader and W. A. J. Dalton, Polarization dependence of EM-scattering from Rayleigh scatterers embedded in a dielectric slab—2. Experiment, *J. Appl. Phys.* **46**(10), 4386–4391 (1975).
18. D. C. Look, H. F. Nelson, A. L. Crosbie and R. L. Dougherty, Two-dimensional multiple scattering: comparison of theory with experiment, *Trans. ASME* **100**, 480–485 (1978).
19. R. W. Spinrad, J. Ronald, V. Zaneveld and H. Pak, Volume scattering function of suspended particulate matter at near-forward angles: a comparison of experimental and theoretical values, *Appl. Optics* **17**(7), 1125–1130 (1978).
20. J. Janzen, Extinction of light by highly nonspherical strongly absorbing colloidal particles: spectrophotometric determination of volume distributions for carbon blacks, *Appl. Optics* **19**(17), 2977–2985 (1980).
21. D. C. Look, H. F. Nelson and A. L. Crosbie, Anisotropic two dimensional scattering: comparison of experiment with theory, *ASME J. Heat Transfer* **103**, 127–134 (1981).
22. H. F. Nelson, Angular distribution of radiation scattering: comparison of experiment and theory, *AIAA J.* **19**, 412–414 (1981).
23. H. F. Nelson, Radiative scattering cross-sections: comparison of experiment and theory, *Appl. Optics* **20**(3), 500–504 (1981).
24. E. Battistelli, P. Bruscaglioni, A. Ismaelli, L. Lo Porto and G. Zaccanti, Separation and analysis of forward scattered power in laboratory measurements of light beam transmittance through a turbid medium, *Appl. Optics* **25**(3), 420–430 (1986).
25. H. F. Nelson, D. C. Look and A. L. Crosbie, Two dimensional radiative back scattering from optically thick media, *ASME J. Heat Transfer* **108**, 619–625 (1986).
26. S. A. W. Gerstl, A. Zardecki, P. W. Unruh, D. M. Stupin, G. H. Stokes and N. E. Elliott, Off-axis multiple scattering of a laser beam in turbid media: comparison of theory with experiment, *Appl. Optics* **26**(5), 779–785 (1987).
27. H. F. Nelson and B. V. Satish, Transmission of a laser beam through anisotropic scattering media, *J. Thermophys. Heat Transfer* **1**(3), 233–239 (1987).
28. T. R. Marshall, C. S. Parmenter and M. Seaver, Characterization of polymer latex aerosols by rapid measurement of 360° light scattering patterns from individual particles, *J. Colloid Interface Sci.* **55**(3), 624–636 (1976).
29. R. G. Pinnick, D. E. Carroll and D. E. Hofmann, Polarized light scattered from monodisperse randomly oriented aerosol particles: measurements, *Appl. Optics* **15**(2), 384–393 (1976).
30. K. J. Daniel, N. M. Laurendeau and F. P. Incropera, Comparison of predictions with measurements for radiation transfer in an algal suspension, *Int. J. Heat Mass Transfer* **21**, 1379–1384 (1978).
31. K. G. Privoznik, K. J. Daniel and F. P. Incropera, Absorption, extinction and phase function measurements for algal suspensions of *Chlorella Pyrenoidosa*, *J. Quant. Spectrosc. Radiat. Transfer* **20**, 345–352 (1978).
32. F. P. Incropera and K. G. Privoznik, Radiative property measurements for selected water suspensions, *Water Resour. Res.* **15**(1), 85–89 (1979).
33. M. Bartholdi, G. C. Salzman, R. D. Hiebert and M. Kerker, Differential light scattering photometer for rapid analysis of single particles in flow, *Appl. Optics* **19**(10), 1573–1581 (1980).
34. S. A. Boothroyd, R. A. Jones, K. W. Nicholson and R. Wood, Light scattering by fly ash particles and the applicability of Mie theory, *Combust. Flame* **69**, 235–241 (1987).
35. H. F. Nelson and B. V. Satish, Radial scattering of a laser beam in anisotropic scattering media, *J. Thermophys. Heat Transfer* **2**(2), 104–109 (1988).
36. Duke Scientific Corporation Bulletin, California (1983).
37. J. V. Dave, *IBM J. Res.* **13**, 302 (1969).
38. H. C. van de Hulst, *Light Scattering by Small Particles*. Dover, New York (1981).
39. F. Bohren and D. R. Huffman, *Absorption and Scattering of Light by Small Particles*. Wiley, New York (1983).
40. M. P. Mengüç and S. Subramaniam, A step phase function approximation for the experimental determination of the effective scattering phase functions for particles,

J. Quant. Spectrosc. Radiat. Transfer **43**(3), 253–265 (1990).
41. E. Hecht, *Optics*, 2nd Edn. Addison-Wesley, New York (1988).
42. J. H. Joseph, W. J. Wiscombe and J. A. Weinman, The delta-Eddington approximation for radiative flux transfer, *J. Atmos. Sci.* **33**, 2452–2459 (1976).
43. M. F. Modest and F. H. Azad, The influence and treatment of Mie-anisotropic scattering in radiative heat transfer, *J. Heat Transfer* **102**, 92–98 (1980).
44. A. L. Crosbie and G. W. Davidson, Dirac-delta function approximations to the scattering phase function, *J. Quant. Spectrosc. Radiat. Transfer* **33**, 391–409 (1985).

ANALYSE PROGRESSIVE ET INVERSE DE LA DIFFUSION SIMPLE OU MULTIPLE DU RAYONNEMENT COLLIMATE DANS UN SYSTEME AXISYMETRIQUE

Résumé—On étudie la diffusion d'une source de lumière collimatée incidente sur un milieu axisymétrique à diffusion simple ou multiple et on détermine la possibilité d'extension de cette analyse pour couvrir les propriétés radiatives effectives du milieu. Pour cela un nephelomètre laser He–Ne est conçu et les distributions angulaires de luminance diffusée sont mesurées dans des régions de diffusion simple ou multiple pour des suspensions mono (ou poly) dispersées de particules. Des expressions analytiques sont obtenues pour la distribution angulaire de luminance. Les expériences montrent un bon accord avec les calculs théoriques. Une analyse inverse est aussi présentée pour déterminer les coefficients de la fonction de phase des particules *in situ* en utilisant les résultats expérimentaux. Les deux premiers coefficients du développement de Legendre de la fonction de phase sont retrouvés à la fois pour les mono (et poly) dispersions à 10% de la valeur réelle des expériences conduites avec des épaisseurs optiques faibles ($\tau < 0{,}5$).

UNTERSUCHUNG DER EINFACH- UND MEHRFACH-STREUUNG VON GERICHTETER STRAHLUNG IN EINEM ACHSENSYMMETRISCHEN SYSTEM

Zusammenfassung—In dieser Arbeit wird die Streuung von gerichtetem Licht an einem einfach/mehrfach streuenden achsensymmetrischen Medium untersucht. Dabei kommt es besonders darauf an festzustellen, ob auf diese Weise die effektiven Strahlungseigenschaften des Mediums ermittelt werden können. Zu diesem Zweck wird unter Verwendung eines He–Ne-Lasers ein Streuungsmeßgerät gebaut, womit dann die Winkelabhängigkeit der Streuungsintensität in Bereichen der Einfach- und Mehrfach-Streuung an mono- und polydispersen Partikelsuspensionen bestimmt werden. Für die winkelabhängige Verteilung der Intensität werden analytische Ausdrücke ermittelt, die bis zu drei aufeinanderfolgende Streuvorgänge berücksichtigen. Experimentelle Befunde und theoretische Berechnungen stimmen sehr gut überein. Darüberhinaus wird ein inverses analytisches Verfahren zur "*in-situ*"-Bestimmung der Phasenfunktions-Koeffizienten der Partikel aufgrund der Versuchsergebnisse vorgestellt. Die beiden ersten Koeffizienten der Legendre-Entwicklung der Phasenfunktion werden sowohl für Mono- als auch für Polydispersionen innerhalb 10% des tatsächlichen Wertes (aus Experimenten bei geringer optischer Dicke ($\tau < 0{,}5$)) ermittelt.

ПРЯМОЙ И ОБРАТНЫЙ АНАЛИЗ ЕДИНИЧНОГО И МНОЖЕСТВЕННОГО РАССЕЯНИЯ КОЛЛИМИРОВАННОГО ИЗЛУЧЕНИЯ В ОСЕСИММЕТРИЧНОЙ СИСТЕМЕ

Аннотация—Исследуется рассеяние коллимированного излучения, падающего на осесимметричную среду с единичным/множественным рассеянием, и определяется возможность использования его анализа для восстановления эффективных излучательных свойств среды. С этой целью разработан лазерный нефелометр He–Ne и измерены распределения интенсивности углового рассеяния в режимах единичного и множественного рассеяния для моно- и полидисперсных взвесей частиц. Получены аналитические выражения для распределения интенсивности углового рассеяния, учитывающие до трех последовательных рассеяний. Экспериментальные данные очень хорошо согласуются с теоретическими расчетами. Предложен обратный анализ для определения коэффициентов фазовой функции частиц *in situ* на основе экспериментальных данных. Два первых коэффициента в разложении Лежандра для фазовой функции рассчитаны как для моно-, так и для полидисперсии в пределах 10% от действительной величины в случае проведения экспериментов при малой оптической толщине ($\tau < 0{,}5$).